Available online at www.sciencedirect.com
SCIENCE DIRECT®
International Journal of Heat and Mass Transfer 47 (2004) 925–936
International Journal of HEAT and MASS TRANSFER
www.elsevier.com/locate/ijhmt

New model for frost growth rate

Byeongchul Na [1], Ralph L. Webb *

Department of Mechanical Engineering, The Pennsylvania State University, 206 Reber Building, University Park, PA 16802, USA

Received 10 May 2003; received in revised form 28 August 2003

Abstract

Many models have been published to predict frost growth. These may be divided into empirical and theoretical models. All prior theoretical models assume the water vapor is saturated at the interface between the air stream and frost layer. This paper provides a new theoretically based numerical model of frost deposition and growth. The present model: (1) uses supersaturated water vapor at the frost surface, which is fundamentally correct; (2) improved correlations for frost thermal conductivity; (3) uses a rationally based tortuosity factor; and (4) calculates the local frost density variation. For numerical simulation of the frost growth rate, the measured thermal conductivity was used. Frost growth rate on a cold surface was measured, and the experimental data were compared to the numerical model and agreed within 15%. The proposed supersaturation model was also compared to previous investigators' experimental data, and it was found that the supersaturation model is superior to analytical or numerical models that assume the water vapor at the frost surface to be saturated.

1. Introduction

The frost layer is a porous structure composed of ice crystals and air pores. Because the porous structure contains low thermal conductivity air pores, the frost layer has low thermal conductivity. Therefore, this layer results in a significant heat transfer resistance from the air to the evaporator surface. The frost layer on an evaporator has finite thickness, and it acts to restrict the air flow. This blockage causes the air pressure drop to increase, and the balance point for the system-fan characteristic curve changes as the frost layer grows, reducing the air flow rate. Thus, the increase of heat transfer resistance caused by frost layer and the reduced air flow rate degrades the evaporator performance. A more precise analysis procedure of the frost growth rate is required to improve the prediction of the evaporator performance. The prediction of the frost growth rate is related to the mass transfer rate from the air stream to the frost layer, mass diffusion rate within the frost layer, and thermal conductivity of the frost layer. Particularly, the mass transfer rate from the air stream to the frost layer is the most important parameter because it directly affects the frost growth rate. The main issues of this paper are to address calculation of the mass transfer rate and how the mass transfer rate affect the frost growth rate.

Barron and Han [1] and Brian et al. [2,3] assumed that the water vapor is saturated at the frost surface in their calculation of the mass transfer rate from the air stream to the frost layer. They determined the water vapor saturation pressure using the saturation curve for water vapor over ice. This assumption has been used by many other researchers, such as Sanders [4], Tokura et al. [5], Le Gall and Grillot [6], Sami and Duong [7], Jones and Parker [8], Lee et al. [9], Tao et al. [10], and Schneider [11]. Mao et al. [12] developed an empirical correlation for the mass transfer coefficient during frost growth; however, this correlation is based on the cold surface temperature (not on the frost surface temperature). Na and Webb [13–15] have shown that the air is supersaturated at the frost surface, as opposed to the previous assumptions that the water vapor is saturated at the frost surface. The supersaturated conditions are defined by the supersaturation degree at the frost surface defined by

* Corresponding author. Tel.: +1-814-865-0283; fax: +1-814-865-1344.
E-mail addresses: bxn6@psu.edu (B. Na), r5w@psu.edu (R.L. Webb).
[1] Tel.: +1-814-865-9719; fax: +1-814-865-1344.

0017-9310/$ - see front matter © 2003 Elsevier Ltd. All rights reserved.
doi:10.1016/j.ijheatmasstransfer.2003.09.001

Nomenclature

c_p	specific heat (kJ/kg K)
D_v	water vapor diffusion coefficient (m/s)
D_{eff}	effective water vapor diffusion coefficient in the frost layer defined in Eq. (8) (m/s)
h	heat transfer coefficient (W/m^2 K)
i_{sv}	sublimation energy of water (kJ/kg)
k	thermal conductivity (W/m K)
K_w	mass transfer coefficient based on humidity ratio difference (kg/m^2 s)
m''_v	water vapor mass flux (kg/m^2 s)
m''_{vd}	water vapor mass flux by molecular diffusion rate (kg/m^2 s)
$m''_{v,thick}$	mass transfer rate contributing frost layer thickness growth (kg/m^2 s)
P_v	vapor pressure (kPa)
P_{vs}	saturated vapor pressure (kPa)
q''	heat flux (W/m^2)
RH	relative humidity
S	supersaturation degree $[(P_v - P_{vs})/P_{vs}]$ as defined by Eq. (1) (dimensionless)
T	temperature (°C)
t	time (s)
V	velocity (m/s)
W	humidity ratio
x	coordinate along the frost thickness (m)
x_{fs}	frost layer thickness (m)
Greek symbols	
ρ	density (kg/m^3)
τ	tortuosity factor
ξ_{fr}	weighting factor defined in Eq. (14)
Subscripts	
a	air
exp	experimental value
fr	frost layer
fs	frost surface
ice	ice
pre	predicted value
sen	sensible heat
v	vapor
w	cold surface
∞	free stream

$$S \equiv (P_v - P_{vs})/P_{vs} \quad (1)$$

Na and Webb [15] proved that the frost is supersaturated at the surface by experiments and by theoretical analysis. Also, Na and Webb provide a simple equation for the supersaturation degree at the frost surface that was that predicted their experimental data. Na and Webb [15] used their "supersaturation model" to predict the mass transfer rate at the frost layer. This paper uses the supersaturation model in their new frost growth model, and the predicted results are compared to the authors' experimental data and to previously published data.

Na and Webb [15] showed that moderate uncertainty in the tortuosity factor has very small effect on the heat transfer rate through the frost layer and frost densification rate if one uses rational correlations for the mass diffusion prediction within the frost layer. Thus, Prager correlation will be used for predicting the frost growth rate, which is discussed in [15].

O'Neal and Tree [16] provided a comprehensive review of the correlations for thermal conductivity of the frost layer. They note that each correlation was developed for a certain temperature range. The ice crystal shape, which affects the heat conduction path through the frost layer, is dependent on the temperature. The present authors provide a new equation for the thermal conductivity of the frost layer based on the morphology of the ice crystals. This correlation used for the prediction of the frost growth rate.

2. Frost growth mechanism

Fig. 1a shows the physical model of frost layer growth. Sensible heat is transferred from the air to the frost surface by the temperature difference driving force between the air stream and frost surface. Water vapor is also transferred from the air stream to the frost surface by the concentration difference driving force between the air stream and the frost surface. Some of the transferred moisture deposits on the frost layer, causing the frost layer to grow. The remainder diffuses into the frost layer. The heat of sublimation caused by the phase change of the added frost layer is transferred through the frost layer. This latent heat and the sensible heat transferred from the air are then transferred through the frost layer by conduction. The water vapor diffusing into the frost layer changes phase within the frost layer, leaving the latent heat within the frost layer. This latent heat is transferred by conduction within the frost layer. The frost density increases as a result of this process. This is described as the "densification process."

2.1. Mathematical formulation of model

The mathematical formulation of the frost growth, densification, and heat and mass transfer on the frost surface and within the frost layer is developed by control volume analysis. Fig. 1b shows the differential control

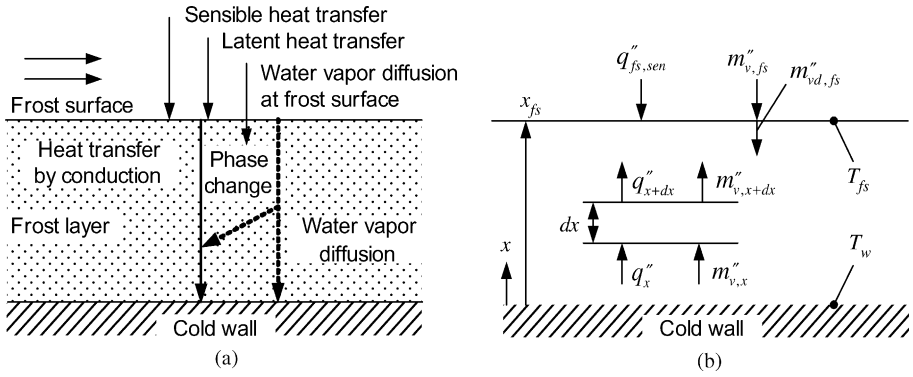

Fig. 1. Frost growth model: (a) physical model, (b) mathematical model.

volume in the frost layer. The sensible heat transfer rate on the frost surface may be expressed as

$$q''_{\text{sen}} = h(T_{\text{a}} - T_{\text{fs}}) \tag{2}$$

The transferred mass flux of water vapor from the air to the frost surface is

$$m''_{\text{v}} = K_{\text{w}}(W_{\text{a}} - W_{\text{fs}}) \tag{3}$$

where W_{fs} is the humidity ratio of the moist air at the frost surface. The mass transfer from the air causes an increase of the frost thickness and increases the density of the frost layer. This may be expressed as

$$m''_{\text{v,fs}} = m''_{\text{v,thick}} + m''_{\text{vd,fs}} \tag{4}$$

$$m''_{\text{thick}} = \rho_{\text{fs}}(\mathrm{d}x_{\text{fs}}/\mathrm{d}t) \tag{5}$$

$$\rho_{\text{fs}}(\mathrm{d}x_{\text{fs}}/\mathrm{d}t) = m''_{\text{v,fs}} - m''_{\text{vd,fs}} \tag{6}$$

The water diffusion at the frost surface into the frost layer is calculated by

$$m''_{\text{vd,fs}} = -D_{\text{eff}}\rho_{\text{a}}\mathrm{d}(\rho_v/\rho_{\text{a}})/\mathrm{d}x|_{x=x_{\text{fs}}} \tag{7}$$

The effective molecular diffusion coefficient (D_{eff}) is introduced in Eq. (7). The effective molecular diffusion coefficient considers the tortuous diffusion path and the restricted diffusion area and is defined as [15]

$$D_{\text{eff}} = \tau\varepsilon_{\text{fr}}D_{\text{v}} \tag{8}$$

The frost layer becomes more dense by the deposition of the water vapor within the frost layer. The densification rate is related to the water vapor diffusion rate within the frost layer, which is related to the tortuosity [15]. The governing equations for the densification of the frost layer, and the heat and mass transfer through the frost layer are presented in this section. The boundary and initial conditions for the differential equations are also discussed. For simplicity, these phenomena are treated as a one-dimensional transient process. This approach may be extended to two or three-dimensional problems without difficulty.

As the water vapor diffuses through the frost layer, it changes its phase to ice on the existing frost crystals. This mechanism takes place continuously, while the frost density increases with time. Using the mass conservation law, the relation of the frost density change rate and mass transfer within the frost layer may be expressed as

$$\partial\rho_{\text{fr}}/\partial t = -\partial m''_{\text{vd}}/\partial x \tag{9}$$

The symbol ρ_{fr} is the local density of the frost layer and is expressed as

$$\rho_{\text{fr}} = \varepsilon_{\text{fr}}\rho_{\text{a}} + (1 - \varepsilon_{\text{fr}})\rho_{\text{ice}} \tag{10}$$

where ε_{fr} is the local porosity of the frost layer, ρ_{ice} is the density of the ice, and ρ_{a} is the density of the moist air in the frost layer. The existing frost density (ρ_{fr}) is dependent on time. Using the definition of the effective diffusion coefficient, the molecular diffusion rate, m''_{vd} in the frost layer is expressed by Fick's law:

$$m''_{\text{vd}} = -D_{\text{eff}}\rho_{\text{a}}\mathrm{d}(\rho_{\text{v}}/\rho_{\text{a}})/\mathrm{d}x \tag{11}$$

Using Eqs. (9) and (11), the local densification rate of the frost layer becomes

$$\frac{\partial\rho_{\text{fr}}}{\partial t} = \frac{\partial}{\partial x}\left(D_{\text{eff}}\rho_{\text{a}}\frac{\mathrm{d}(\rho_{\text{v}}/\rho_{\text{a}})}{\mathrm{d}x}\right) \tag{12}$$

Two boundary conditions for the water vapor density and an initial condition for the frost density are required to solve Eq. (12). One boundary condition is obtained from the analysis of the initial condition of the frost growth and densification, and the other boundary condition is obtained from the conditions at the frost surface. The initial frost density will be discussed in the next section.

Considering energy conservation in the control volume, the two mechanisms of energy transfer are:

(1) sensible heat transfer by conduction through the frost layer;
(2) latent heat transfer due to phase change of the water vapor on the frost crystals.

The energy conservation equation is in the form of

$$\frac{\partial}{\partial x}\left(k_{\mathrm{fr}}\frac{\partial T_{\mathrm{fr}}}{\partial x}\right)+i_{\mathrm{sv}}\frac{\partial \rho_{\mathrm{fr}}}{\partial t}=\rho_{\mathrm{fr}}c_{\mathrm{p,fr}}\frac{\partial T_{\mathrm{fr}}}{\partial t} \tag{13}$$

where i_{sv} is the sublimation enthalpy of the water vapor, and k_{fr} and $c_{\mathrm{p,fr}}$ are the thermal conductivity and specific heat of the frost, respectively. The specific heat of the frost is obtained from the density or porosity of the frost layer by

$$c_{\mathrm{p,fr}}=[\rho_{\mathrm{ice}}(1-\varepsilon_{\mathrm{fr}})c_{\mathrm{p,ice}}+\rho_{\mathrm{a}}\varepsilon_{\mathrm{fr}}c_{\mathrm{p,a}}]/\rho_{\mathrm{fr}} \tag{14}$$

Eq. (13) requires two boundary conditions for the frost temperature. One is the cold surface temperature, and the other is the frost surface temperature, which is related to the heat and mass transfer at the frost surface.

2.2. Boundary and initial conditions

The mathematical model discussed in the previous section requires specification of the boundary conditions at the cold surface and the frost surface, and the initial conditions for the frost density and temperature. In this section, the boundary conditions and initial condition will be discussed.

Boundary conditions. The boundary conditions for the temperature are

$$T_{\mathrm{fr}}=T_{\mathrm{w}} \quad \text{where } x=0 \tag{15a}$$

$$T_{\mathrm{fr}}=T_{\mathrm{fs}} \quad \text{where } x=x_{\mathrm{fs}} \tag{15b}$$

The cold surface temperature T_{w} is prescribed value, and the frost surface temperature T_{fs} is linked to the heat and mass transfer resistances of the air-side convection and conduction and diffusion through the frost layer. Thus, using prescribed air-side conditions (temperature, humidity, and velocity) and frost properties (thermal conductivity, density, and tortuosity factor), the frost surface temperature may be calculated.

Some of the water transferred onto the frost surface from the air stream diffuses into the frost layer and the remaining adds to the frost layer thickness. In order to calculate the frost growth rate, the density of the accumulated frost must be known. The analytical models of Brian et al. [2,3] and Jones and Parker [8] assume that the density of the fresh frost is same as the average density of the frost layer. Thus, they did not account for the density variation within the frost layer. The Tao et al. [10] numerical model assumed that the gradient of the frost density at the frost surface is zero. They gave no justification for this assumption. Le Gall and Grillot [6] set the frost surface density at a fixed value (25 kg/m^3), but did not justify use of this value. With successive water vapor deposition on the frost surface, the deposition sites will be identical to the previous deposition sites, which cause the gradient of the frost density at the frost surface to be zero. The present model uses this specification.

In order to solve the frost growth rate and heat transfer across the frost layer, initial conditions for the frost thickness, density, and temperature are required. The initial temperature can be taken as the cold surface temperature, if the initial frost thickness is so thin that the heat transfer resistance of the initial frost thickness is negligible compared to the air side heat transfer resistance.

Jones and Parker [8] tested the initial conditions by changing the values of the initial frost thickness and density and found that:

- Initial thickness can approach zero ($\approx 2\times 10^{-5}$ m) without causing significant problems in predicting the frost growth rate.
- As long as the initial value of the frost density is significantly smaller than the frost density during growth, it will not affect the solution for the frost growth rate and densification.

Jones and Parker [8] evaluated the effect of the initial value of the frost density on the frost growth rate and densification in their model by changing the value from 8 to 48 kg/m^3. They found that the frost density and thickness converged to the same value in a few minutes. Based on their investigation, the initial value of the frost density can be taken as any value within 8–48 kg/m^3. In this work, the initial conditions for the frost temperature, thickness, and will be fixed as follows:

- Temperature: $T_{\mathrm{fr}}=T_{\mathrm{w}}$
- Thickness: $x_{\mathrm{fs}}=2\times 10^{-5}$ m
- Density: 30 kg/m^3

2.3. Mass transfer at the frost layer

Experiments of Na and Webb [15] showed that water vapor is supersaturated at the frost surface. This was further validated using the laminar boundary layer analysis. By regression of the analytical data, the following simple equation for the supersaturation degree at the frost surface was developed:

$$S_{\mathrm{fs}}=0.808(P_{\mathrm{v},\infty}/P_{\mathrm{vs},\infty})(P_{\mathrm{vs,fs}}/P_{\mathrm{vs},\infty})^{-0.657}-1 \tag{16}$$

$$T_{\mathrm{fs}}+14\ ^{\circ}\mathrm{C}<T_{\infty}<T_{\mathrm{fs}}+20\ ^{\circ}\mathrm{C} \quad \text{and} \quad -40\ ^{\circ}\mathrm{C}<T_{\mathrm{fs}}<0\ ^{\circ}\mathrm{C}$$

This work uses Eq. (16) to determine the humidity ratio at the frost surface for calculation the mass transfer rate from the air stream to the frost surface. Using Eqs. (1) and (16), the water vapor pressure at the frost surface is

calculated. Using the calculated water vapor pressure and the ideal gas equation, the water vapor density is calculated, and this water vapor density is converted to the humidity ratio at the frost surface to calculate the mass transfer rate using Eq. (3).

2.4. Thermal conductivity of the frost layer

Based on results from other studies, Kobayashi [17] cataloged the shape of frost crystals and assimilated the results in his "Temperature-Excess vapor density diagram" shown in Fig. 2a. Kobayashi used the term, "excess vapor density" instead of the supersaturation degree. The excess vapor density is defined by the difference between the vapor density of the air and the saturated vapor density at a given temperature. According to his diagram, the principal factors affecting the crystal shape are the air temperature and the supersaturation degree.

The morphology of the crystals is dependent on the temperature and supersaturation degree. For different frost crystal shapes, the thermal conductivities may be different, because of the different heat conduction path. The frost layer is a porous medium composed of air pores and ice crystals, and the low air thermal conductivity results in low frost thermal conductivity. Thus, the amount of the air pores (represented by the porosity of the frost layer) is an important factor in determining the thermal conductivity of the frost layer.

(1) Fig. 2b shows the microscopic structure of ice crystal and the main shapes were discussed [18]. Summarizing

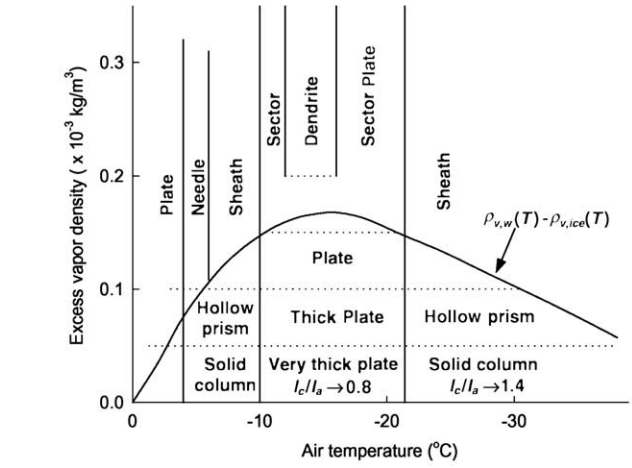

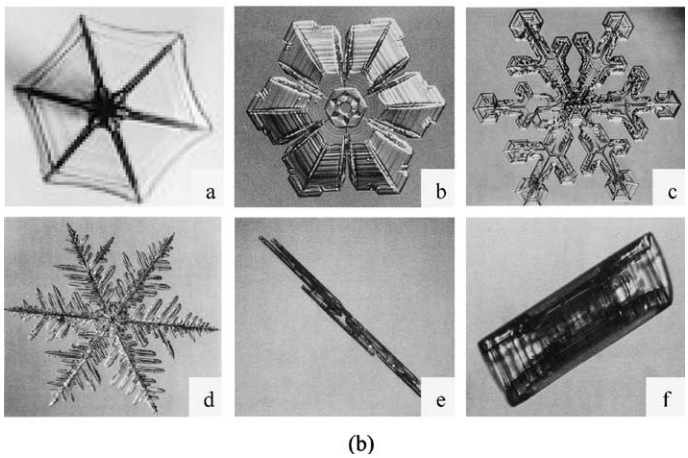

Fig. 2. Morphology of ice crystal. (a) Diagram showing the snow crystal forms depending on excess vapor density and air temperature [17]. (b) Ice crystal shape [18]—(1) Plate-like forms: (a) plate, (b) simple sectored plate, (c) dendritic sectored plate, (d) fern-like stellar dendrite; (2) Column-like forms: (e) needle crystal, (f) hollow column, or sheath-like crystal.

the frost morphology [17]: Ice crystal shapes are classified into two main forms: plate-like forms and column-like forms.

(2) These main forms are dependent on the temperature at which ice crystals are generated.

(3) Variants on the two main forms are influenced by the supersaturation degree of the water vapor.

The main shapes and their variants are shown in Fig. 2b, and the effect of temperature and supersaturation are shown in Fig. 2a. The thermal conductivity is mainly dependent on the heat conduction path through the frost crystals. Examining the frost crystal shapes in Fig. 2b, one concludes that the heat conduction path is related to the main forms (plate-like or column-like) and these two forms are related to the temperature at which the frost crystals are generated. Thus, it is expected that the thermal conductivity of the frost layer may be different in the following regions:

- Region 1: −4 to −10 °C Column-like forms
- Region 2: −10 to −21 °C Plate-like forms
- Region 3: −21 °C Column-like forms

Based on the above classification, the desired test range and conditions were established. Table 1 shows the range in which the tests for the frost thermal conductivity were conducted in this work. The temperature region between 0 and −4 °C will be ignored in the discussion, because this temperature region is rare in the refrigeration systems of interest in this work.

For the reasons discussed in the previous section, the effect of the supersaturation degree can be excluded here. Thus, the correlation for frost thermal conductivity will be developed in the three defined different temperature ranges that affect the basic frost crystal shapes.

Fig. 3a shows the experimental data for the frost thermal conductivity. The temperature ranges, for which the data were taken, are given on Fig. 3a. The general characteristic is that the thermal conductivity of the frost layer increases as the frost density increases, as expected. However, each data set, which was taken in different temperature ranges, shows a different dependency on the frost density. This is because the frost crystal shapes are dependent on the temperature, at which the crystals are generated, and that the shape affects the heat transfer path along the frost crystals.

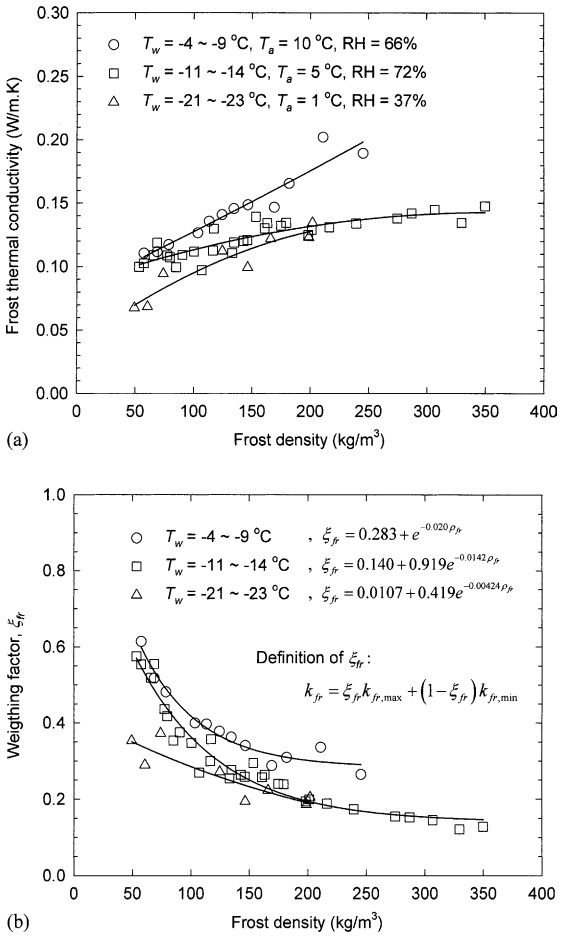

Fig. 3. Thermal conductivity of the frost layer: (a) thermal conductivity of frost layer; (b) weighting factor for frost thermal conductivity.

The thermal conductivity of the frost layer can be expressed in terms of the two limiting models [4] (parallel model and serial model), which give the maximum and minimum thermal conductivity of the frost layer:

$$k_{\mathrm{fr}} = \xi_{\mathrm{fr}} k_{\mathrm{fr,max}} + (1 - \xi_{\mathrm{fr}}) k_{\mathrm{fr,min}} \tag{17}$$

The maximum value $k_{\mathrm{fr,max}}$ and the minimum value $k_{\mathrm{fr,min}}$ can be calculated using the models given in [4]. The

Table 1
Test conditions

	T_a (°C)	T_w (°C)	W_a
Region 1	2.8–10.3	−4.8 to −9.5	0.0028–0.0053
Region 2	0.0–5.9	−18.0 to −11.0	0.0025–0.0043
Region 3	−1.1–1.3	−27.1 to −21.9	0.0013–0.0015

symbol ξ_{fr} in Eq. (17) is the weighting factor. This weighting factor is related to the morphology of the frost crystals. Fig. 3b shows the weighting values determined from the experimental data for the frost thermal conductivity and the $k_{fr,max}$ and $k_{fr,min}$, which are calculated at the test conditions and frost density. Using a regression method, the following equations were obtained for the weighting factors in different temperature ranges:

$$\text{Region 1:}\quad \xi_{fr} = 0.283 + e^{-0.020\rho_{fr}} \qquad T_w : -4 \text{ to } -10\ ^\circ\text{C} \tag{18a}$$

$$\text{Region 2:}\quad \xi_{fr} = 0.140 + 0.919e^{-0.0142\rho_{fr}} \qquad T_w : -10 \text{ to } -21\ ^\circ\text{C} \tag{18b}$$

$$\text{Region 3:}\quad \xi_{fr} = 0.0107 + 0.419e^{-0.00424\rho_{fr}} \qquad T_w : -21\ ^\circ\text{C} \tag{18c}$$

Examining Fig. 3b, the weighting factor decreases as the frost density increases. The mechanism causing the frost density increase is the diffusion of the water vapor within the frost layer and deposition on the frost crystals. The direction of the frost crystal growth within the frost layer, which is responsible for the densification of the frost layer, is relatively normal to the surface on which the frost grows. The frost thermal conductivity approaches the value calculated using the serial model in [4]. The trend shown in Fig. 3b is in good agreement with the above qualitative analysis.

This correlation was developed based on the present experimental data. The measured temperature difference between the frost surface and wall was in the range of 1.5–2.5 °C for the frost thermal conductivity measurements. Because this temperature difference is small, the wall temperature was taken as the representative temperature of the frost layer in developing the correlation. This is more convenient in applications, because neither the frost surface temperature nor the frost layer temperature is directly available to calculate the frost thermal conductivity. It is desirable to check the validity of the correlation by comparing its ability to predict the thermal conductivity data measured by the other investigators. Fig. 4a–c shows the validity of the correlation

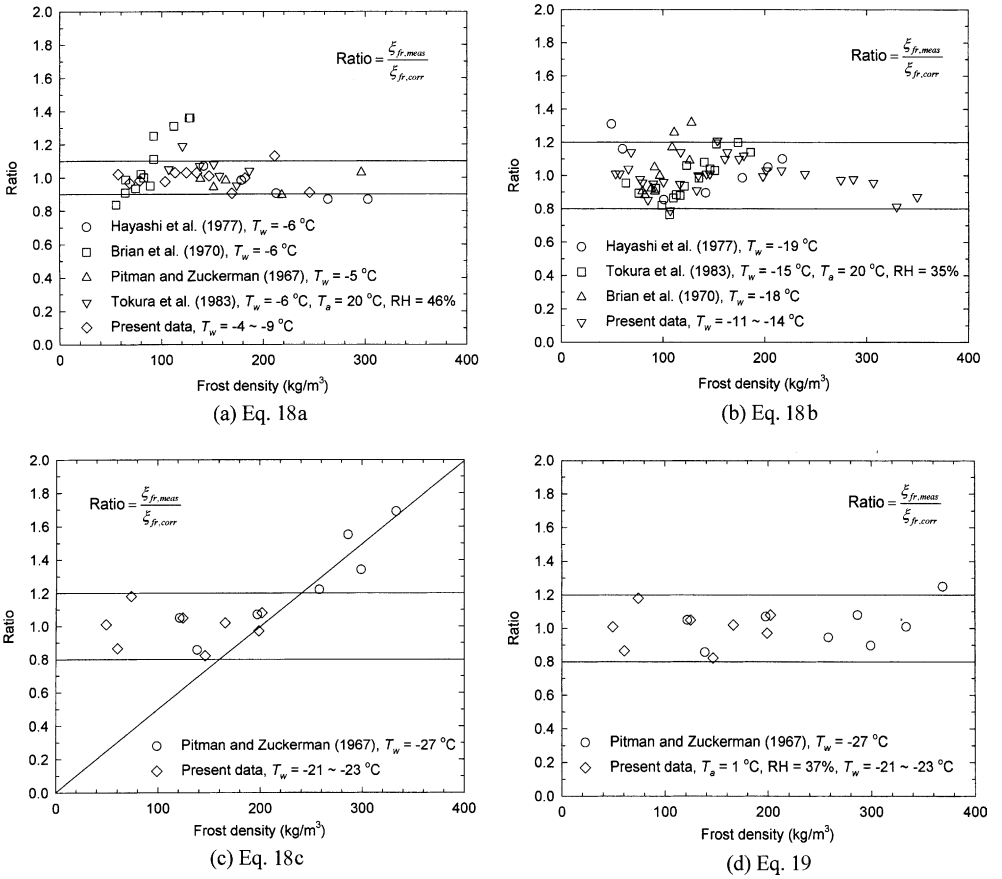

Fig. 4. Comparison of experimental data to correlation.

developed in this work. The published data were measured in the temperature range of 0 to −40 °C, which is of interest in this work. In Region 1 and Region 2, the correlation predicts all of the data shown in Fig. 4a and b within ±20%. However, in Region 3, Eq. (18c) does not show good agreement with the Pitman and Zukerman [19] data at the higher density than 200 kg/m^3. In order to improve the prediction of the high density Pitman and Zukerman data, Eq. (18c) can be modified to

$$\xi_{fr} = 0.0107 + 0.419e^{-0.00424\rho_{fr}}, \quad \rho_{fr} < 200\ \text{kg/m}^3 \text{ and } T_w < -21\ ^\circ\text{C} \tag{19a}$$

$$\xi_{fr} = 0.005\rho_{fr}\left(0.0107 + 0.419e^{-0.00424\rho_{fr}}\right), \quad \rho_{fr} > 200\ \text{kg/m}^3 \text{ and } T_w < -21\ ^\circ\text{C} \tag{19b}$$

Fig. 4d shows that Eq. (19) can predict the experimental data within ±20% for the thermal conductivity in Region 3.

Summarizing the analysis of the thermal conductivity:

(1) The density of the frost layer is related to the frost growth rate. Therefore, the frost density must be related to the frost growth rate, which depends on the environmental conditions and the mass transfer coefficient of the frost surface.

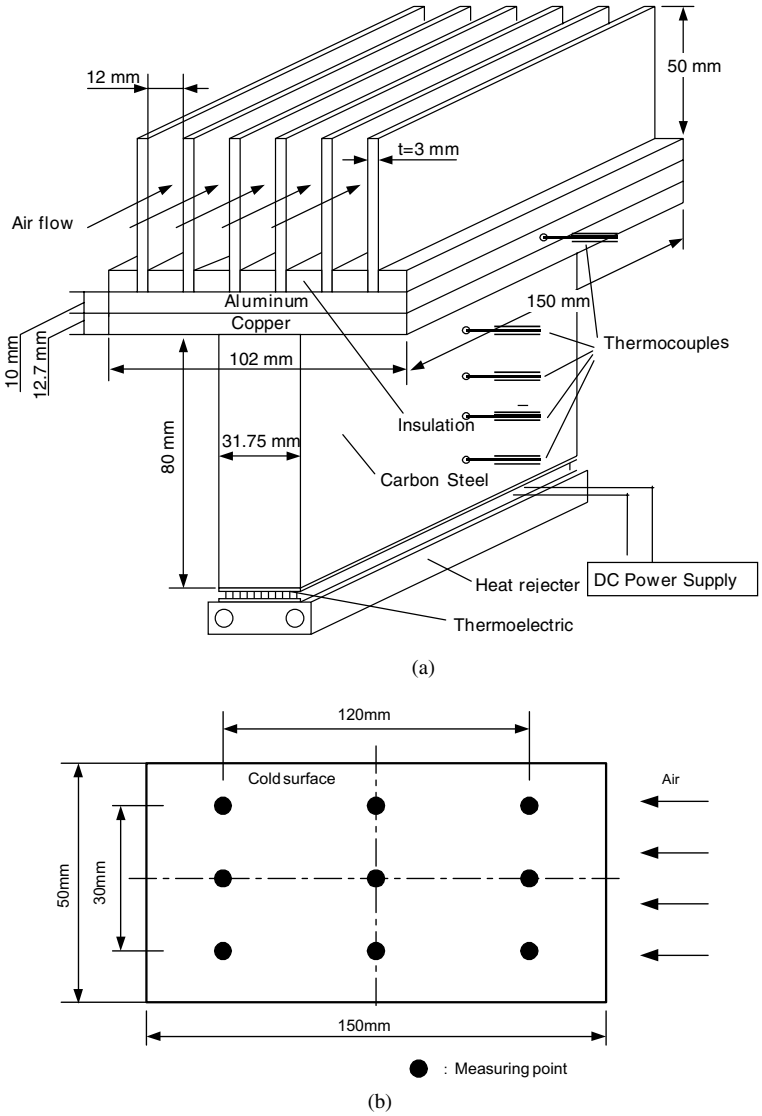

Fig. 5. Experimental setup: (a) test section; (b) measuring points for frost thickness.

(2) The thermal conductivity of the frost layer depends on the frost temperature. The developed correlation for the frost density spans −4 to −27 °C and agrees within ±20% of the published data.

3. Experiment for frost growth rate

To compare the proposed new frost growth model to the experimental data, the frost growth rate was measure for different environment conditions. The test surface was fabricated of pure aluminum as shown in Fig. 5a. This design is composed of six aluminum fins on the aluminum base to increase the heat transfer area. The heat transfer from the air occurs only on the fins. This test surface was located on the cold block shown in Fig. 5a. The carbon steel block is cooled by the thermoelectric modules driven by a DC power supply. The heat on the hot side of the thermoelectric modules is removed by coolant flowing through the heat sink. The temperature of the cold block is controlled by the temperature of the coolant.

Different methods have been used to measure the frost thickness. Using a low energy laser beam source, Mao et al. [12] and Besant et al. [20] measured the frost layer thickness. The laser beam was aligned parallel to the frost surface. The laser beam was moved normal to the frost surface, and the position of the laser beam, where the laser beam scattered, was detected by a light meter. Sanders [4] used a light slit for measuring the frost layer thickness. The light slit was reflected on the frost surface, and projected on the opposite side of the light slit source. The frost thickness was measured by monitoring the projected beam. In the present work, we tested these methods and found that the laser beam scattering was too great to define the frost surface position, and the reflection of a light beam generates a large spot of projection due to the rough frost surface. Hence, it is difficult to define the exact point indicating the frost thickness in the large projected light spot. Therefore, the frost thickness was directly measured by a micrometer having a 0.025 mm resolution. For specified air velocity, inlet humidity, and cold surface temperature, the frost layer grows on the cold surface. At every 10–30 min, the frost layer thickness was measured at nine points. These measuring points are shown in Fig. 5b. The values measured at the nine points were averaged to define the frost layer thickness.

4. Results and discussion

Two variants of the present model are evaluated in this work. These will be referred to as the "saturation model" and the "supersaturation model." These differ in whether the vapor is assumed saturated at the frost surface (saturation model) or the supersaturated at the frost surface (supersaturation model). As previously stated, we believe the supersaturation model to be fundamentally correct, as compared to the saturation model used by previous researchers.

The mathematical model was numerically solved using grid sizes between 0.01 and 0.1 mm. Grid sizes below 0.05 mm showed converged result within 0.1%.

Fig. 6a compares the frost growth rate predicted by the present supersaturation model to the experimental data taken in this work. The figure shows very good agreement between the predictions and the data. If the "saturation model" were used to predict the Fig. 6 data, the frost growth rate would be over predicted by approximately 35%. Fig. 6b shows the error between the predicted and experimental data. The error is less than ±15%. Examination of Fig. 6 shows that the model slightly underpredicts the frost growth rate at the early stage of the frost growth and slightly overpredicts the

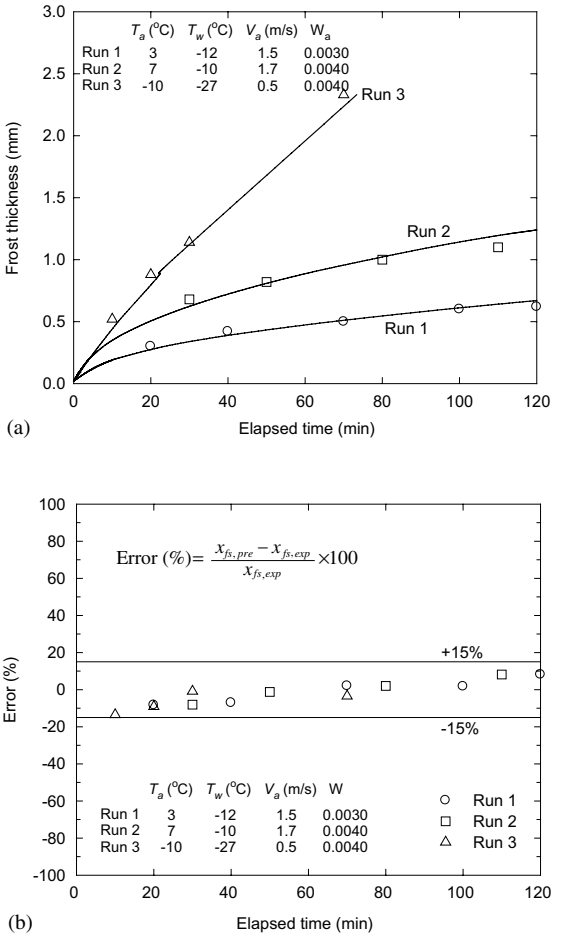

Fig. 6. Comparison of the model to the experimental data: (a) frost growth rate; (b) error between prediction and test result.

data at later time. The under prediction in the early frost growth period may be because the low frost density has a very rough surface compared to the later frost growth period. A rougher surface likely has a higher mass transfer coefficient than on a less rough surface. Thus, the error changes with frost thickness.

Fig. 7a shows the ability of the two variants of the present model to predict the Jones and Parker [8] data. These variants are the "supersaturation model" used for Fig. 6 prediction, and the "saturation model" as defined above. Fig. 7a shows that: (1) the saturation model over predicts the data approximately 50%, and (2) the supersaturation model provides good agreement with the data. The saturation model overpredicts the mass transfer rate from the air stream to the frost surface, and this results in higher frost growth rate than shown by the experimental data. The figure also shows the Jones and Parker model, which assumes no density variation through the frost thickness and saturated water vapor at the frost surface. The Jones and Parker [8] model significantly underpredicts their own data. Jones and Parker state that their model underpredicts their data by 35%. However, they did not explain or speculate why their model underpredicts their experimental data.

The Jones and Parker [8] model has two deficiencies: (1) the assumption of uniform frost density, and (2) assumption of saturated water vapor at the frost surface. The frost growth rate is influenced by the density variation within the frost layer, as discussed in Section 2. Fig. 8 shows an example of the density distribution predicted by the present supersaturation model. Typically, the average frost density is larger than the frost density at the frost surface, and this causes the frost growth rate to be underpredicted. The underpredicted frost thickness causes the average frost density to be overpredicted, and the error is accumulated. This may be a reason the Jones and Parker model underpredicts their experimental data approximately 35%.

Fig. 7b shows the data of Sanders [4] and predictions using the present supersaturation and saturation model

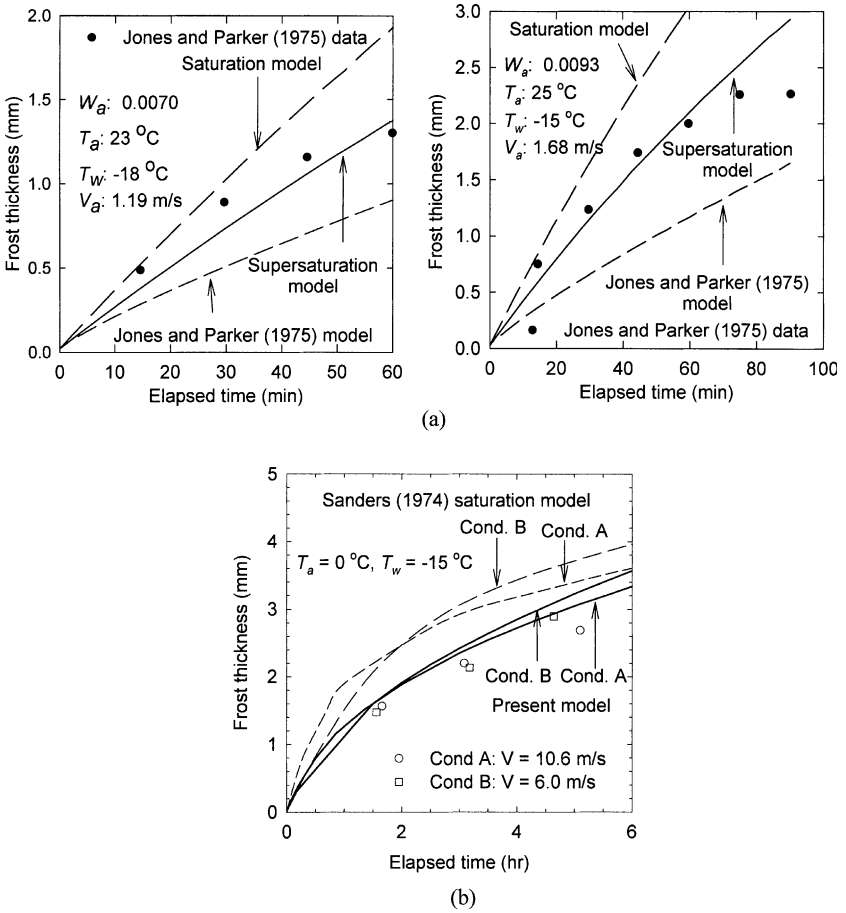

Fig. 7. Comparison of the model to published data: (a) Jones and Parker data; (b) Sanders data [4].

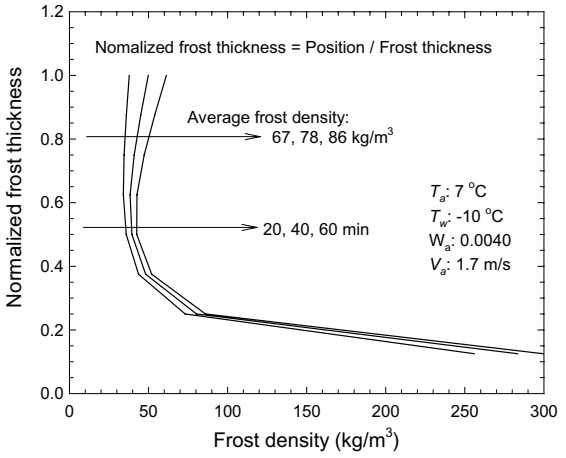

Fig. 8. Density distribution in the frost layer.

variants. The figure shows that the present supersaturation model provides very good prediction of the Sanders data. However, the saturation model substantially over predicts the frost growth rate. The over prediction of the saturation model is because it overpredicts the mass transfer rate from the air stream to the frost surface as discussed in [15]. It is noted that the Sanders data were taken with turbulent flow. The predictions of the present model used the heat transfer coefficient at the frost surface measured by Sanders [4].

Tao et al. [10] and Le Gall and Grillot [6] used a saturation model and compared their predicted results to their experimental data. They adjusted the tortuosity factor to force agreement of their model predictions to the experimental data. This resulted in a tortuosity factor greater than 1.0, which is physically impossible as discussed in [15]. When the tortuosity factor is arbitrarily increased, the mass diffusion rate at the frost surface and within the frost layer will increase, and this depresses the frost growth rate. Based on the present work, their treatment of the tortuosity factor is implausible.

The ability of the present supersaturation model to predict the frost growth rate for three independent data sources provides strong support of the validity of the model.

Na and Webb [15] showed that the assumption of the saturation at the frost surface overpredicts the mass transfer rate by the factor of 4–30 in their test range. The present work shows that assumption of saturation at the frost surface results in approximately 30% over prediction of the frost thickness. As the frost growth rate increases, the frost surface temperature decreases due to the increase of the thermal resistance through the frost layer. Use of the saturation model will result in a higher than actual frost surface temperature, and will decrease the predicted mass transfer rate.

5. Conclusions

(1) This work provides strong evidence that the air is supersaturated at the frost surface, as opposed to the assumption of saturated air used in previously published frost growth models.
(2) A new model is formulated that is based on supersaturated air at the frost surface, accounts for density variation in the frost layer, and uses an improved correlation for frost thermal conductivity.
(3) The present supersaturation model shows very good ability to predict the frost growth rate for three independent data sources.
(4) If one assumes saturated air at the frost surface, this variant of the present model will over predict the frost growth rate approximately 30%.
(5) The density variation within the frost layer clearly affects the frost growth rate, and the uniform frost density Jones and Parker model [8] underpredicts the frost growth rate.
(6) Some previously published models that use an empirical tortuosity factor greater than 1.0 are physically unrealistic.

References

[1] R.F. Barron, L.S. Han, Heat and mass transfer to a cryosurface in free convection, J. Heat Transfer 87 (4) (1965) 499–506.
[2] P.L.T. Brian, R.C. Reid, I. Brazinsky, Cryogenic frost properties, Cryog. Technol. 5 (1969) 205–212.
[3] P.L.T. Brian, R.C. Reid, Y.T. Shah, Frost deposition on cold surfaces, Ind. Eng. Chem. Fundam. 9 (3) (1970) 375–380.
[4] C.T. Sanders, The influence of frost formation and defrosting on the performance of air coolers, Ph.D. Thesis, Delft Technical University, 1974.
[5] I. Tokura, H. Saito, K. Kishinami, Study on properties and growth rate of frost layers on cold surfaces, J. Heat Transfer 105 (1983) 895–901.
[6] R. Le Gall, J.M. Grillot, Modeling of frost growth and densification, Int. J. Heat Mass Transfer 40 (13) (1997) 3177–3187.
[7] S.M. Sami, T. Duong, Mass and Heat Transfer during Frost Growth, in: ASHRAE Transactions, vol. 95 (part 1), 1989, pp. 158–165.
[8] B.W. Jones, J.D. Parker, Frost formation with varying environmental parameters, J. Heat Transfer 97 (1975) 255–259.
[9] K.S Lee, W.S. Kim, T.H. Lee, A one-dimensional model for frost formation on a cold flat surface, Int. J. Heat Mass Transfer 40 (18) (1997) 4359–4365.
[10] Y.X. Tao, R.W. Besant, K.S. Rezkallah, A mathematical model for predicting the densification and growth of frost on a flat plate, Int. J. Heat Mass Transfer 36 (2) (1993) 353–363.
[11] H.W. Schneider, Equation of the growth rate of frost forming on cooled surface, Int. J. Heat Mass Transfer 21 (1978) 1019–1024.
[12] Y. Mao, R.W. Besant, H. Chen, Frost Characteristics and Heat Transfer on a Flat Plate under Freezer Operating

Conditions, in: ASHRAE Transactions, No. 4295, 1999, pp. 231–251.
[13] B. Na, Analysis of frost formation on an evaporator, Ph.D Thesis, The Pennsylvania State University, 2003.
[14] B. Na, R.L. Webb, A fundamental understanding of factors affecting frost nucleation, Int. J. Heat Mass Transfer 46 (2003) 3797–3808.
[15] B. Na, R.L. Webb, Mass transfer on and within a frost layer, Int. J. Heat Mass Transfer, in press.
[16] D.L. O'Neal, D.R. Tree, A Review of Frost Formation in Simple Geometries, in: ASHRAE Transactions, vol. 91, 1985, pp. 267–281.
[17] T. Kobayashi, T. Kuboda, in: I. Sungagawa (Ed.), Snow Crystals, Morphology of Crystals, Terra Scientific Publishing Company, Tokyo, 1987, pp. 649–743.
[18] http://www.its.caltech.edu/~atomic/snowcrystals/primer/primer.htm.
[19] D. Pitman, B. Zuckerman, Effective thermal conductivity of snow at −88, −27, and −27 °C, J. Appl. Phys. 38 (1967) 2698–2699.
[20] R.W. Besant, K.S. Rezkallah, Y. Mao, J. Falk, Measurement of Frost Thickness Using a Laser Beam and Light Meter, in: ASHRAE Transactions, vol. 96 (part 1), No. 3361, 1990.